International Journal of Heat and Mass Transfer 52 (2009) 1223–1229

Contents lists available at ScienceDirect

International Journal of Heat and Mass Transfer

journal homepage: www.elsevier.com/locate/ijhmt

Model of a porous regenerator used for magnetic refrigeration at room temperature

Jonathan Bouchard [a], Hakim Nesreddine [b,*], Nicolas Galanis [a]

[a] Université de Sherbrooke, 2500 Boulevard de l'Université, Sherbrooke (QC), Canada J1K 2R1
[b] Hydro-Québec, Laboratoire des technologies de l'énergie, 600 Avenue de la Montagne, Shawinigan (QC), Canada G9N 7N5

ARTICLE INFO

Article history:
Received 27 November 2007
Received in revised form 18 August 2008
Available online 7 November 2008

Keywords:
Porous regenerator
Magnetocaloric effect
Magnetic refrigeration
CFD

ABSTRACT

A transient three-dimensional model of a porous regenerator operating at room temperature is presented. The solid magnetic material and the regeneration fluid are modeled separately. The fluid flows through interstitial channels formed by a regular matrix of solid particles. The velocity, pressure and temperature fields are obtained from the simultaneous solution of the Navier–Stokes and energy equations with variable properties in the solid and the Boussinesq approximation for the fluid. The magnetocaloric effect (MCE) is taken into account by the inclusion of a source term in the energy equation for the magnetic solid. Special numerical schemes are used to avoid unrealistic computation time and memory requirements. Typical velocity fields and transient temperature profiles are presented.

1. Introduction

The temperature rise of a magnetic material generated by the application of a magnetic field, the magnetocaloric effect (MCE), was first observed by Warburg in 1881 [1]. Debye later developed the basis of the magnetic refrigeration (MR) cycle to attain cryogenic temperatures [2]. In the mid 70's, Brown proved MR could work at ambient temperatures by generating a temperature difference of 47 K with a ferromagnetic refrigerant. More recently, the MR prototypes often operate near ambient temperature and follow a process known as active magnetic regeneration (AMR) proposed by Barclay [3]. The AMR cycle comprises four processes. During the magnetization, the magnetic field is applied to the ferromagnetic refrigerant resulting in an increase of its initial temperature due to the MCE. Maintaining the field, fluid flow regenerates the solid and rejects the MCE heat towards a warm sink. Next, the field is deactivated resulting in a temperature drop of the solid refrigerant induced by the MCE. Because of the preceding regeneration process, the solid temperature is now lower than it was at the start of the cycle. Finally, fluid flows in the opposite direction regenerating the solid and allowing heat addition from a cold source. Astronautics Corporation of America [4,5] and Chubu Electric Power [6] research teams presented similar MR prototypes. They both use porous regenerator beds assembled on a wheel rotating in and out of a magnetic field generated by a permanent magnet. Gadolinium or gadolinium alloys particles are filling the regenerator beds. Other prototypes put emphasis on versatility of the design such as the works of Bohigas et al. [7] and Clot et al. [8]. Their prototypes are constructed in a modular fashion and use permanent magnets and gadolinium thin sheets.

The regenerator usually reaches steady state operation after several MR thermodynamic cycles are completed. In this state, it displays a quasi linear temperature profile in opposition to the uniform initial temperature distribution. Therefore, the regenerator displays a cold end and a hot end depending on fluid flow direction. For optimum efficiency, the mean regenerator temperature must be close to the solid Curie temperature for which the MCE is maximum. Because of this aspect, the latest MR prototypes display layered regenerator beds of multiple ferromagnetic solids chosen in such a way that their Curie point follows the regenerator temperature profile [9,10].

Because of the complexity of the regenerator operation, its performance cannot be assessed with accuracy. As a consequence, the global efficiency of a MR system can only be approximately estimated. Data regarding thermal behavior of the regenerator is gathered from measurements on MR prototypes. The regenerator is usually considered as a black box characterized by the entrance and exit states of the fluid. The internal temperature distribution of the regenerator is rarely measured. Clot et al. [8] performed such measurements with a regenerator made of thin gadolinium sheets.

The measured data is useful, but specific to a prototype. Numerical simulations are more general and allow the quantification of the hydrodynamic and thermal phenomena taking place within the regenerator. The few regenerator models presented so far in the literature [11,12] are all of the same type. They are transient one dimensional effective models. The internal flow through the porous magnetic material is replaced by an external flow around a consolidated solid of simple geometry. The fluid velocity of this external flow is considered uniform and is computed from the imposed mass flow. Hence, the flow field is uncoupled from the

* Corresponding author. Tel.: +1 819 539 1400 ext. 1414; fax: +1 819 539 1409.
E-mail address: nesreddine.hakim@lte.ireq.ca (H. Nesreddine).

0017-9310/$ - see front matter © 2008 Elsevier Ltd. All rights reserved.
doi:10.1016/j.ijheatmasstransfer.2008.08.031

Nomenclature

B	magnetic field density (T)
B_U	Brillouin function
c_p	specific heat (J/kg K)
F	body force (m/s^2)
G	Lande factor
H	magnetic field intensity (A/m)
H_0	external field intensity (A/m)
H_m	molecular field intensity (A/m)
k	thermal conductivity (W/m K)
k_B	Boltzmann constant (J/K)
M	magnetization (A/m)
N	particle number
n	normal direction
N_d	demagnetization factor
p	pressure (Pa)
S_S	energy source (W/m^3)
S_M	magnetic entropy (J/kg K)
S_L	lattice entropy (J/kg K)
S_E	electronic entropy (J/kg K)
t	time (s)
Δt	time step (s)
T	temperature (K)
T_c	Curie temperature (K)
T_D	Debye temperature (K)
ΔT_{ad}	Magnetocaloric effect MCE (K)
U	net atomic spin component
V	Velocity (m/s)

Greek symbols

η	energy ratio
γ	electronic c_p coefficient (J/kg K^2)
λ	MFA constant (T^2/J)
μ	magnetic permeability (H/m)
μ_B	Bohr magneton (J/T)
μ_r	relative permeability
μ_0	free space permeability (H/m)
ν	kinematic viscosity (m^2/s)
φ	scalar magnetic potential (A)
ρ	density (kg/m^3)

Subscripts

f	fluid
i	section number
in	inside
n	time interval
s	solid
y	flow direction

temperature field and only the energy equations in the fluid and in the solid are solved. Effective physical properties of the solid are described via the porosity parameter. Heat exchange between the fluid and solid phases is obtained from a Nusselt number correlation defined as a function of Reynolds and Prandtl numbers. When considered, pressure drop across the regenerator is modeled using a friction factor correlation. The resulting equations are usually solved for the unknown fluid and solid temperatures using the finite difference method on a two-dimensional space-time grid.

The results generated by these models, although valuable, show discrepancies with experimental data. The differences are mainly caused by the use of the heat transfer correlation and the over simplification of the porous geometry. Also, the disregard of the interaction between the flow and temperature fields impacts the heat exchange between phases. To eliminate the use of heat transfer and pressure drop correlations, the velocity, pressure and temperature fields must be solved simultaneously. In doing so, a porous geometry close to reality has to be modeled. Because of the dependence of the MCE on temperature and the transient character of the problem, the regenerator cannot be simulated as a single representative cell. Its full extend must be modeled, at least in the flow direction. The numerical solution requires time to implement and important computation power. This explains the simplified model formulations presented so far in the literature.

In this paper we present a new model for the description of the transient flow and temperature fields in a parallelepipedic MR regenerator filled with small gadolinium particles. It is based on the three-dimensional Navier–Stokes equations for the fluid flow around these discrete particles which are alternatively heated and cooled during magnetization and demagnetization. The adopted numerical solution is explained and typical results are presented and analysed.

2. Model description

2.1. Regenerator geometry

The dimensions of the prototype parallelepipedic regenerator under construction are 25, 50 and 100 mm in the x, z and y directions respectively. The fluid flows in the positive y direction during magnetization and in the opposite direction during demagnetization. A group of channels are formed by stacking particles in the regenerator volume. Two constraints dictate the particles shape in the adopted model. First, to be true to the prototype, the regenerator porosity must display an adjustable value between 40% and 50%. Second, the meshing tools produce poor quality meshes when half or quarter particles are present. As a consequence, only full particles must be stacked. Because of this, cubic centered, cubic face centered or hexagonal compact structures do not allow the minimum target porosity to be attained. Instead, the porous matrix is built with a combination of ellipsoids and spheres. The spheres are positioned in the interstices of adjacent ellipsoids as shown in Fig. 1 which depicts a small portion of the entire regenerator. The xOy and yOz planes are parallel to the walls of the regenerator which is made up by a juxtaposition of several such portions. The mean particle diameter is 0.5 mm. Stacked at full capacity, the porosity of this regenerator is 33%.

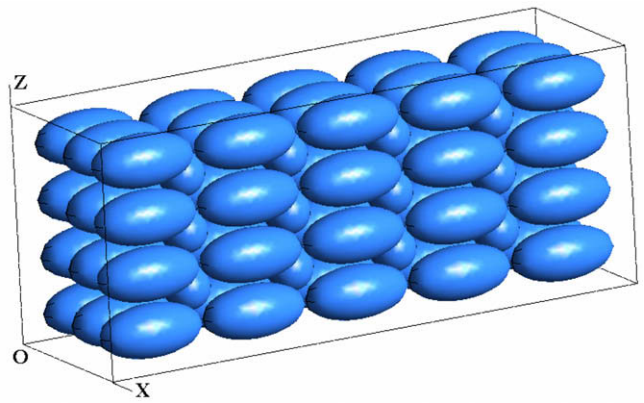

Fig. 1. Schematic representation of a portion of the porous regenerator.

2.2. Mathematical formulation

In this section, a general methodology to describe the detailed transient operation of a ferromagnetic regenerator under nonzero magnetic field is presented. It includes three distinct groups of equations: the hydrodynamic and energy equations for the fluid, the energy equation for the solid particles and the magnetic field equations. Because the fluid is considered incompressible the continuity and momentum equations are as follows:

$$\vec{\nabla}\cdot\vec{V} = o \tag{1}$$

$$\frac{\partial\vec{V}}{\partial t} + (\vec{V}.\vec{\nabla})\vec{V} = \vec{F} - \frac{1}{\rho_f}\vec{\nabla}p + \nu\vec{\nabla}^2\vec{V} \tag{2}$$

where V is the velocity, F the body force, p the pressure, ρ_f the fluid density and ν the fluid kinematic viscosity. Turbulence closing equations are not needed. Indeed, the fluid flow is sufficiently low speed to be treated as laminar. The flow is single-phased and there is no surface tension since the ferromagnetic solid is always surrounded by the regenerator fluid, even when not cycling, to avoid oxidation. Hence, capillary forces induced by adhesion and cohesion are irrelevant to the present model and, therefore, gravity is the only body force considered. The application of Boussinesq's hypothesis implies that the density in the expression of this force is temperature dependent. If viscous dissipation is neglected due to low mass flow, the temperature of the fluid obeys the following energy equation:

$$\rho_f(c_p)_f\left(\frac{\partial T_f}{\partial t} + \vec{V}\cdot\vec{\nabla}T_f\right) = k_f\vec{\nabla}^2T_f \tag{3}$$

where T_f, c_p and k_f are respectively the fluid temperature, specific heat and thermal conductivity.

In addition, the temperatures of the regeneration fluid and the magnetic solid are closely related. The variation of the external magnetic field generates the MCE which elevates or lowers the temperature of the solid. Hence, the fluid and solid temperatures are constantly evolving during the course of MR cycles. The MCE temperature variation ΔT_{ad} is transformed into an energy density and included in the energy equation for the solid [13]:

$$\rho_s c_p(H,T_s)\frac{\partial T_s}{\partial t} = k_s\vec{\nabla}^2T_s + S_s(H,T_s) \tag{4}$$

$$S_s = \frac{\rho_s c_p(H,T_s)\Delta T_{ad}(H,T_s)}{\Delta t} \tag{5}$$

where H is the magnetic field intensity, T_s, ρ_s, k_s and $c_p(H,T_s)$ the temperature, density, thermal conductivity and specific heat of the solid. The term S_s is a source (positive) during magnetization and a sink (negative) during demagnetization. The special treatments required for the computation of the specific heat of the solid and the MCE temperature variation ΔT_{ad} is presented in the next section.

Finally, magneto-static theory can be used to determine the field intensity within the ferromagnetic material. In the absence of real currents, scalar magnetic potential formulation may be applied [14]. The gradient of this potential corresponds to the magnetic field intensity.

$$|\vec{H}| = -|\vec{\nabla}\phi| \tag{6}$$

The magnetic potential φ is obtained from the following equation:

$$\vec{\nabla}\cdot[\mu_r(H,T_s)\vec{\nabla}\phi] = 0 \tag{7}$$

The relative magnetic permeability μ_r is generally not spatially uniform. Therefore, the magnetic field intensity will vary within the solid. Hence, the resulting MCE temperature variation will be dependent on position and the energy source will also vary within the solid. The rate of heat transfer between the solid and the fluid, already not uniform because of convection heat transfer, will surely be additionally affected by the magnetic field non-uniform spatial distribution.

The magnetic potential, the magnetic field intensity, the temperatures of the solid and the fluid, the fluid velocity components and the fluid pressure form a system of eight unknowns governed by Eqs. (1)–(7). They must be solved simultaneously because of the strong coupling between the magnetic, temperature and velocity fields.

2.3. Properties of the ferromagnetic solid

Except for the magnetic permeability, the specific heat and the MCE, all the other properties of the solid required for the solution of the equations are considered constant. The magnetic permeability of the ferromagnetic solid is obtained from experimental data. Isotherms of magnetization M versus applied field are usually measured for samples such as spheres, disks or cylinders. In those cases, the following simple relationship exists between applied and internal field intensity [15]:

$$|H| = |H_{applied}| - N_d|M| \tag{8}$$

The demagnetization factor N_d in Eq. (8) is a constant which depends on the shape of the sample. Once H is evaluated with Eq. (8) using the applied field and the measured magnetization, Eq. (9) is used to compute the corresponding magnetic permeability. Because sharp variations are typical, two dimensions temperature and field intensity interpolation generates the best magnetic permeability values [13].

$$\mu_r = 1 + M/H \tag{9}$$

The specific heat of the ferromagnetic solid displays a sharp maximum around its Curie temperature. Hence, the statistical physics molecular field approximation (MFA) cannot alone describe adequately this property. The MFA is therefore corrected with the temperature dependent measured specific heat data for zero magnetic field. First, the specific heat is expressed as a function of magnetic S_M, lattice S_L and electronic S_E entropy [16]:

$$c_p(H,T_s) = T_s\left[\frac{\partial S_M(T_s,H)}{\partial T_s} + \frac{\partial S_L(T_s)}{\partial T_s} + \frac{\partial S_E(T_s)}{\partial T_s}\right] \tag{10}$$

Statistical physics provide expressions for each entropy component. The lattice and electronic components are only functions of the temperature:

$$S_L = Nk_B\left[-3\ln\left(1-e^{-(T_D/T_s)}\right) + 12\left(\frac{T_s}{T_D}\right)^3\int_0^{T_D/T_s}\frac{\chi^3}{e^\chi-1}d\chi\right] \tag{11}$$

$$S_E = \gamma T_s \tag{12}$$

where N is the particle number, k_B the Boltzmann constant, T_D the Debye temperature, γ the electronic entropy coefficient and χ an integration variable. The magnetic component is written in terms of the Brillouin function B_U which argument η is the ratio of magnetic and thermal energy.

$$S_M = Nk_B\left[\ln\left\{\frac{\sinh[\eta(U+1/2)]}{\sinh(\eta/2)}\right\} - \eta UB_U(\eta)\right] \tag{13}$$

$$B_U(\eta) = \frac{1}{U}[(U+1/2)\coth[(U+1/2)\eta] - (1/2)\coth(\eta/2)] \tag{14}$$

$$\eta = \frac{g\mu_B(H+\lambda M)}{k_BT_b} \tag{15}$$

With the net atomic spin component U, the Lande factor g, the Bohr magneton μ_B and the MFA constant λ which is a function of U and the exchange integral [16]. This model generates satisfying results

only past the Curie temperature in the paramagnetic region. Below the transition temperature, in the ferromagnetic region, the MFA is corrected with experimental data for $c_p(0,T_s)$. Thus:

$$c_p(H,T_s) = c_p(0,T_s) - T\frac{\partial(S_M(0,T_s) - S_M(H,T_s))}{\partial T_s} \quad (16)$$

The magnetic entropy decreases with increasing field. Hence, the specific heat in zero magnetic field is always greater than in non zero field. Fig. 2 compares the predictions of the corrected and uncorrected specific heat models for gadolinium [13] with the corresponding experimental data measured by Tishin [17].

The MCE temperature variation is computed by the integral Eq. (17) given by Tishin [18]. It emphasises the fact that the MCE is generated by the variation of the magnetic field intensity. The corrected specific heat model is reused to evaluate the integrant. The magnetization is directly derived from the MFA and defined in terms of the Brillouin function presented in Eq. (14).

$$\Delta T_{ad}(\Delta H,T_s) = -\int_{H_1}^{H_2} \frac{T_s}{c_p(H,T_s)}\left(\frac{\partial M(H,T_s)}{\partial T_s}\right)_H dH \quad (17)$$

$$M(H,T_s) = Ng\mu_B UB_U(\eta) \quad (18)$$

The MCE temperature variation displays sharp variations near the Curie temperature. As a consequence, the most robust numerical integration methods are necessary to evaluate this effect. Fig. 3 illustrates the MCE of gadolinium for a 2 T rise or drop of the magnetic field.

2.4. Symmetries, boundary and initial conditions

Since all the regenerator walls are considered to be adiabatic and the solid particles are set in a regular pattern, symmetries are effective across the planes normal to the axes Ox and Oz of Fig. 1. Therefore these planes define a reduced computation domain. The y extent stays equal to the stream wise length of the regenarator, but the x and z extents are respectively equal to three and four mean particle diameters (i.e. 1.5 mm and 2 mm, respectively). This reduced domain allows for smaller computation time and memory requirements. Its walls consist of fluid. Hence, all boundary conditions are defined for the fluid variables. The $z = 0$, $z = 2$, $x = 0$ and $x = 1.5$ mm symmetry planes are assigned with standard boundary conditions (Fig. 4). Since there is no fluid flow through a symmetry plane, the normal velocity is zero. Also, the tangential velocity components and the temperature gradients in the normal direction are zero.

The planes $y = 0$ and $y = 100$ mm are the entrance or the exit for the fluid flow. During magnetization, the fluid enters at the cold end ($y = 0$) and exits at the hot end ($y = 100$ mm). During demagnetization, the fluid flows from the hot end to the cold end. In both cases, the entrance velocity is considered uniform and proportional to the imposed mass flow.

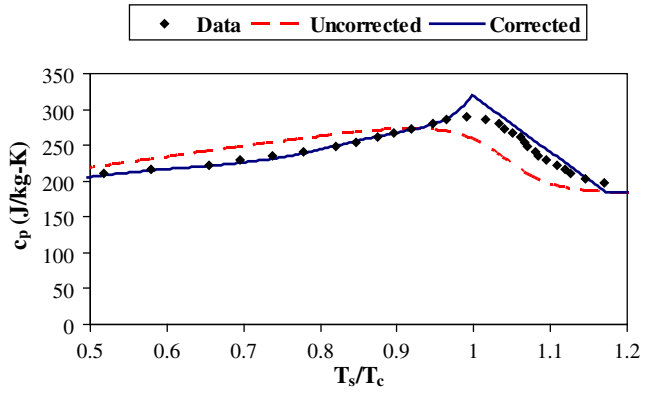

Fig. 2. Specific heat of Gd versus temperature under a constant magnetic field ($B = 2$ T).

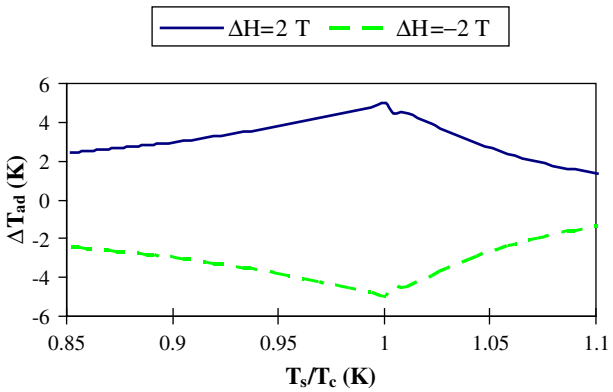

Fig. 3. MCE of Gd versus temperature under a magnetic field variation.

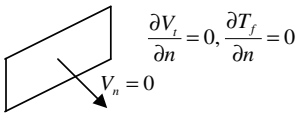

Fig. 4. Symmetry planes boundary conditions.

The fluid entrance temperature is different during magnetization and demagnetization. It is fixed according to MR cycling data. Conservative interface flux is applied at the fluid–solid interface. The heat flux computed on the fluid side of the interface is set equal to the heat flux on the solid side of the interface. The boundary condition for fluid pressure is treated in a standard fashion by fixing the reference pressure at an arbitrary point. It should be noted that boundary conditions at the exit ($y = 100$ mm during magnetization and $y = 0$ during demagnetization) are not necessary since the equations are simplified by neglecting second order axial derivatives at that position. In other terms, the momentum equations are locally parabolic.

A large control volume which surrounds the computation domain is defined to set the magnetic potential boundary conditions as depicted in Fig. 5. The magnetic field at the walls of this large control volume is considered to be undisturbed by the ferromagnetic particles. Hence, a constant and uniform field distribution is effective at the box walls. For example, equipotential XY planes will be created if a uniform field is applied in the z direction as shown in Fig. 5. Near and within the ferromagnetic solid particles, the potential distribution is disturbed altering the field distribution.

At the beginning of the first MR cycle, i.e. before the first magnetization, the initial fluid velocity is set to zero. Also, the solid and

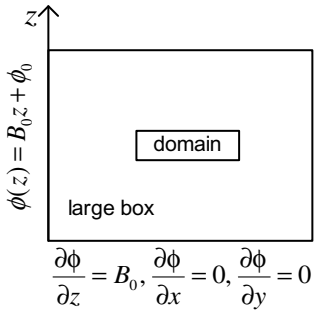

Fig. 5. Scalar magnetic potential boundary conditions.

fluid initial temperatures are set equal. If the initial temperature is uniform, many MR cycles must be simulated to reach the regenerator steady state operation. In order to reduce this initial transient calculation a linear temperature profile between typical temperatures for the cold and hot ends is imposed. All the subsequent resolutions are initialized with the final state of the previous time step.

3. Numerical procedure

The magnetic phenomena of the MCE take place at a much shorter time scale than the thermal effects occurring during the regenerator operation. Hence, the temperature variations induced by the MCE are considered instantaneous in comparison with the ones associated with heat transfer. The MR cycle is then modeled as four sequential steps. First, the magnetization: the magnetic field is applied and generates the MCE x(cf. Fig. 3). Second, fluid flows from the cold to the hot end with the magnetic field still effective. Third, the demagnetization: the magnetic field is removed generating a drop of the solid's temperature (cf. Fig. 3). Finally, fluid flows from the hot to the cold end in zero magnetic field. This MR cycle is repeated with constant frequency.

A time step Δt is chosen for the resolution during the periods of fluid flow. The time step is infinitesimal during the magnetization and demagnetization steps. The source term in the energy equation of the solid displays a high value and generates a fast temperature response. This numerical scheme models the instantaneous nature of the MCE. Also, the source term needs to be linearized in the course of the numerical solution (Eq. (19)). This way, it can be subjected to the same discretization methods applied for the other terms. The S_p component value must always be less than or equal to zero for the numerical solution to be stable [19].

$$S_s = S_u + S_p T_s \tag{19}$$

The coupled system of partial differential equations is solved using the finite volume (FV) methodology. A dense unstructured mesh is used through the computation domain except at the walls of the solid particles. There, regular parallelepiped FV are required for the correct computation of the heat transfer between the solid and fluid phases. The mesh density is chosen after several tests as the minimum required to insure simulation results independency. More than 17 millions FV compose the computation domain. This number exceeds the practical limits of most meshing tools. Hence, as indicated in Fig. 6, the computation domain is divided in 10 sections in the flow direction.

The transient solution of each section is completed one after the other. The order of solution follows the flow direction; sections 1–10 during magnetization and sections 10–1 during demagnetization. Fluid entrance conditions are set for section 1 during magnetization and section 10 during demagnetization. Additional entrance profiles must be defined for all the internal sections. In order to propagate the entrance conditions through the domain, the fluid exit state of one section becomes the entrance state of the next. In addition, the fluid exit state changes at every time step Δt. Hence, the internal sections entrance profiles are constantly updated for each time step. The strategy for section i is illustrated in Fig. 7. The output velocity and temperature distributions of the preceding section at instant $n\Delta t$ are injected as the input for the resolution of section i.

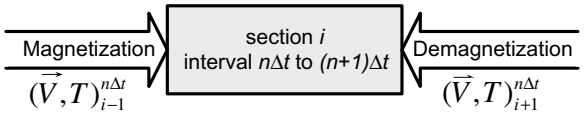

Fig. 7. Internal sections entrance conditions.

This marching solution scheme is valid because the information only propagates in the flow direction. As long as the entrance conditions of the internal sections are updated, the downstream sections can be ignored during the solution process. This fact is validated by comparing two simulations with identical conditions but with different divisions of the domain. One is done on a full section and the other on half a section. The results confirm that the solution in the first half of the full section is identical to that obtained with the half section. This is illustrated in Fig. 8 for the fluid temperature on a typical path in the porous section.

4. Magnetocaloric effect validation

Pure gadolinium particles were stacked in a polymer casing transparent to magnetic field and disposed in between the poles of an electromagnet. Isolated thermocouples are inserted in the porous solid and measure its temperature rise when current circulation activates the effective magnetic field of 0.75 T. As is showed by the measured data presented in Fig. 9, the careful choice of mash technique allowed the gadolinium to fully preserve its ferromagnetic properties. The Curie temperature of the sample was determined to be close to 292.2 K corresponding to standard values [18]. Also, the experimental EMC is in accordance with the EMC rule of thumb values of 2–3 K/T [18]. Fig. 9 also indicates that the EMC generated by the model (Eq. (17)) is in good agreement with the measured data.

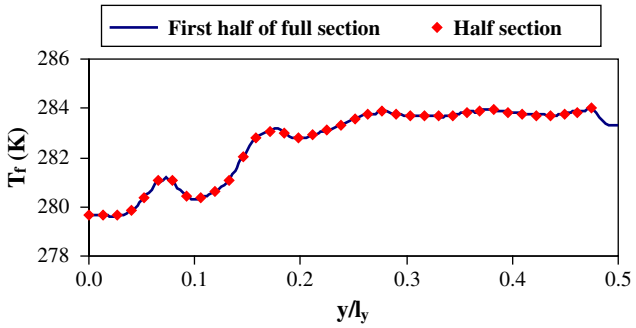

Fig. 8. Marching solution scheme validation.

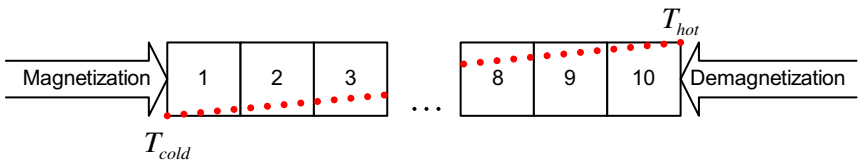

Fig. 6. The computation domain division.

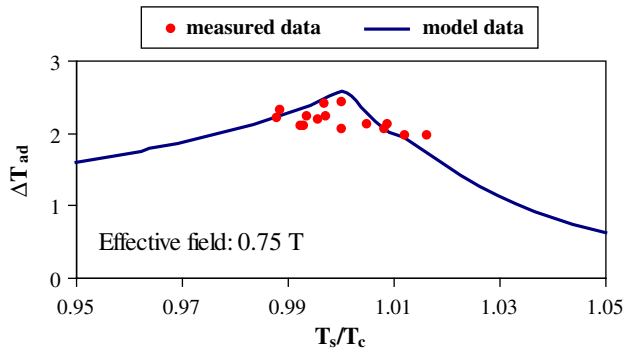

Fig. 9. Experimental validation of Gd magnetocaloric effect.

5. Preliminary results and discussion

Velocity and temperature fields have been calculated for the MR cycle operating conditions presented in Table 1. Water flows in a porous gadolinium matrix. Since the magnetic field is fixed to a constant value, the scalar magnetic potential equation is not solved although the solid specific heat and the MCE are still evaluated as a function of the time varying field and the local temperature Eqs. (16) and (17). To operate in the steady state regime, the initial temperature is set to a linear profile between the fluid entrance temperatures. The fluid is allowed to flow for 6.63 s after the magnetic field application and its removal. Hence, a full cycle is completed in 13.26 s.

The most efficient steady state MR cycle results in the case of complete regeneration. In other words, MCE will always be maximum if the solid initial temperature is restored after the magnetic field variations. Therefore, there exist an explicit relation between the fluid velocity and its residence time within the regenerator that will satisfy this condition. Through multiple trials, such a relation was established for the model. The operating conditions in Table 1 reflect this relation.

Fig. 10a presents a typical velocity field in a plane normal to the x axis at an inner section of the porous domain. The field is well rendered even in the smallest inter-particle channels. The flow field exhibits inertial cores like the ones observed in the flow regimes classification work realized by Dybbs and Edwards [20]. In these cores, typical of the inertial flow regime [20], inertia is the dominant force whereas in the boundary layers, both inertia and viscous forces are important. For the mass flow under consideration, the boundary layers are very close to the particles surface. For the same location as Fig. 10a and b presents the temperature field during the solid regeneration after magnetization. Temperature gradients within particles are visible. Both figures give a good insight into the detailed level of the simulations.

Fig. 11a and b show, respectively, the average solid and fluid bulk temperatures for each of the 10 sections used for the marching solution (c.f. Fig. 6) at different instants during the fluid flow

Table 1
Regenerator operating conditions

Solid material	Gadolinium (Gd)
Fluid	Water
Regenerator porosity	40%
Mass flow rate	2.1 (L/min)
Magnetization entrance temperature	$T_c - 2.5 = 279.17$ (K)
Demagnetization entrance temperature	$T_c + 2.5 = 284.17$ (K)
Magnetic field	2 (T)
Initial temperature	Linear profile
Time for fluid flow	6.63 (s)
Time step for profiles update	1.326 (s)

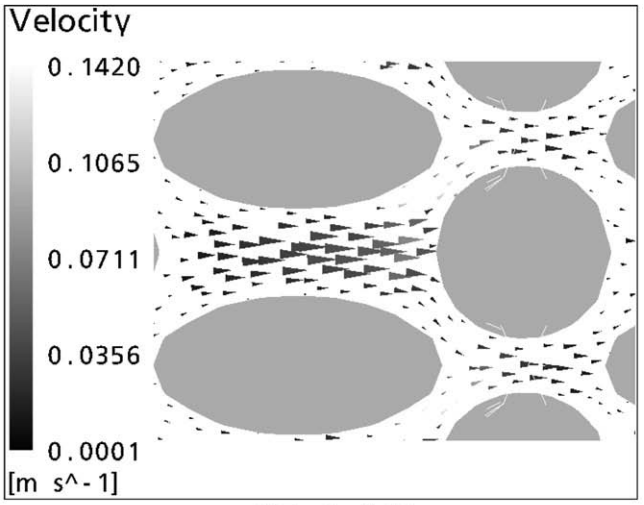

a. Velocity field

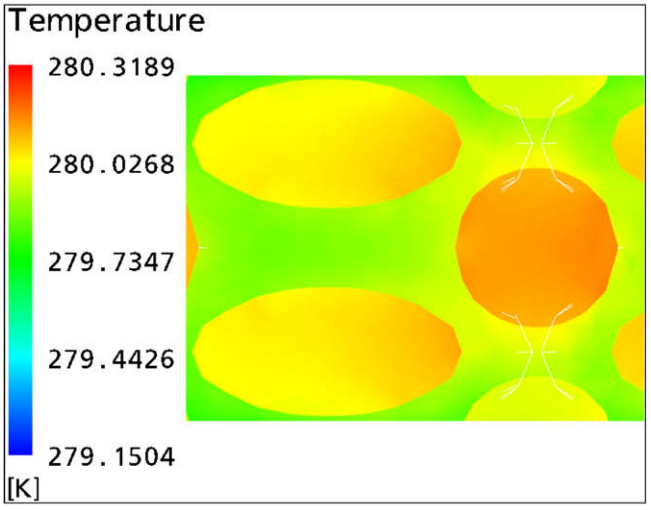

b. Temperature field

Fig. 10. Typical results for operating conditions (Table 1).

from the cold ($y = 0$) to the hot ($y = 100$ mm) end following magnetisation. As expected, both these temperatures increase in the flow direction. When the magnetic field is applied, the temperature of the solid increases from the initial profile ($t = 0$) to the one identified as "magnetization". The colder temperature of the fluid entering the regenerator at $y = 0$ induces a rapid decrease of the solid's temperature. At subsequent instants the temperature difference between the solid and the fluid decreases substantially. It should be noted that the temperature of the solid decreases monotonically with time. At the end of this cooling process (i.e. at $t = 6.63$ s) its temperature is only about 0.15 K higher than its initial temperature. Therefore, the regeneration of the solid is nearly perfect. On the other hand, the bulk temperature of the fluid (Fig. 11b) does not vary monotonically with time. It increase during the initial half of this heat transfer process since the corresponding rate of heat transfer is high in accordance with the large initial temperature difference between the solid and the fluid. Later ($t > 2.652$ s) this temperature difference is small and the rate of heat transfer decreases. Therefore the fluid temperature decreases towards its lowest value which occurs at $t = 6.63$ s.

For the subsequent demagnetization and flow in the opposite direction (i.e. from the hot end at $y = 100$ mm towards the cold end at $y = 0$), the solid and fluid evolutions are similar, but with

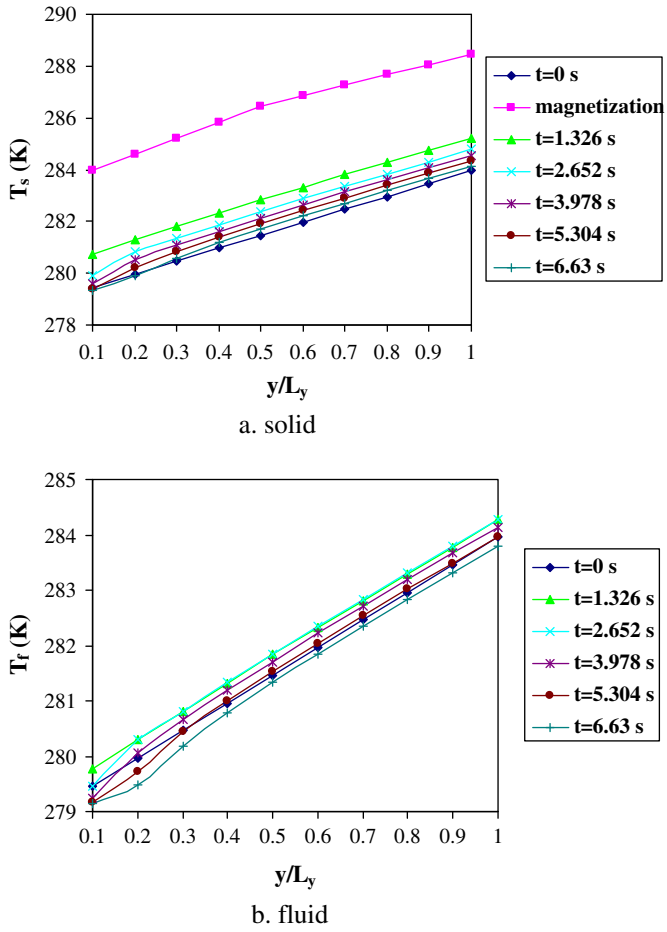

Fig. 11. Temperature profiles during magnetization for operating conditions (Table 1).

temperature variations inverted (the fluid is warmer than the solid particles).

6. Conclusion and future work

A transient three-dimensional model taking into consideration the porous character of a regenerator used for magnetic refrigeration has been successfully developed and solved numerically. It takes into account the coupled effects of the temperature and velocity fields. The solid magnetic particles and the regeneration fluid are modeled separately. The energy equation for the former includes a source term which corresponds to the magnetocaloric effect. The fluid flow through the interstitial channels formed by the solid magnetic particles and the corresponding heat transfer are modeled by the Navier–Stokes and energy conservation equations for the fluid. As far as we can ascertain, this is the first detailed and realistic model for a porous magnetic refrigeration regenerator.

The numerical solution of the system of coupled partial differential equations was obtained using a marching technique and a subdivision of the computation domain into 10 stream wise sections. This approach limits the required computer memory and the CPU time necessary for the simulation of several successive magnetic refrigeration cycles. Typical velocity and temperature field predictions show that the numerical results are quite realistic.

Detailed model results regarding heat transfer and pressure drop as well as the complete description of the regenerator experimental setup and the presentation of the extensive data generated are the subject of upcoming papers.

Acknowledgements

This project is part of the R&D program of the "NSERC Chair in Industrial Energy Efficiency" established in 2006 at Université de Sherbrooke. The authors gratefully acknowledge the support of the Natural Sciences & Engineering Research Council of Canada, Hydro Québec, Rio Tinto Alcan and CANMET Energy Technology Center.

References

[1] E. Warburg, Magnetische untersuchungen, Ann. Phys. Chem. 13 (1881) 141–164.
[2] P. Debye, Einige Bemerkungen zur magnetisierung bei tiefer temperatur, Ann. Phys. Chem. 81 (1926) 1154–1160.
[3] J.A. Barclay, Active and passive magnetic regenerators in gas/magnetic refrigerators, J, Alloys Compd. 207 (1994) 355–361.
[4] C. Zimm, A. Jastrab, A. Sternberg, V. Percharsky, K. Gschneider, M. Osborne, I. Anderson, Description and performance of a near room temperature magnetic refrigerator, Adv. Cryogenic Eng. 43 (1998) 1759–1766.
[5] K. Engelbrecht, G. Nellis, S. Klein, A numerical model of an active magnetic regenerator refrigeration system, Final report 612-10075, Air-Conditioning and refrigeration technology institute, 2005.
[6] N. Hirano, S. Nagaya, M. Takahashi, T. Kuriyama, K. Ito, S. Nomura, Development of magnetic refrigerator for room temperature application, Adv. Cryogenic Eng. 47 (2002) 1027–1034.
[7] X. Bohigas, E. Molins, A. Roig, J. Tejada, X.X. Zhang, Room temperature magnetic refrigerator using permanent magnet, IEEE Trans. Magn. 36 (2000) 538–544.
[8] P. Clot, D. Viallet, F. Allab, A. Kedous-Lebouc, A magnet-based device for active magnetic regenerative refrigeration, IEEE Trans. Magn. 239 (5) (2003) 3349–3351.
[9] C. Zimm, A. Boeder, J. Chell, A. Sternberg, A. Fujita, S. Fujeida, K. Fukamichi, Design and performance of a permanent magnet rotary refrigerator, in: Proceedings of the First International Conference on Magnetic Refrigeration at Room Temperature Systems 3A2, Montreux, 2005, pp.1–7.
[10] N. Hirano, T. Okamura, K. Yamada, S. Nagaya, Performance of a room temperature rotary magnetic refrigerator, International Conference on Magnetic Refrigeration at Room Temperature Systems 2A1, Montreux, 2005, pp.1–6.
[11] K. Engelbrecht, A numerical model of an active magnetic regenerator refrigeration system, Ph.D. Thesis, Wisconsin-Madison University, 2004.
[12] F. Shir, C. Mavriplis, L.H. Bennett, E. Della Torre, Analysis of room temperature magnetic regenerative refrigeration, Intl. J. Refrig. 28 (2005) 616–627.
[13] J. Bouchard, H. Nesreddine, R. Chahine, Impact of demagnetization on magnetocaloric effect in pure gadolinium, 1st International Conference on Magnetic Refrigeration at Room Temperature Materials 1B1, Montreux, 2005, pp. 1–9.
[14] B.I. Bleaney, B. Bleaney, Electricity and Magnetism, Oxford University Press, 1965. p. 147.
[15] S. Chikazumi, Physics of Ferromagnetism, Oxford University Press, 1997. pp. 11–17.
[16] R. Reif, Fundamentals of Statistical and Thermal Physics, McGraw-Hill Inc., 1965. pp. 139–142, 428–431.
[17] A.M. Tishin, Magnetocaloric effect and heat capacity in the phase transition region, Am. Phys. Soc. (1999) 503–511.
[18] A.M. Tishin, Magnetocaloric effect in the vicinity of phase transitions, Handb. Magn. Mater. 12 (1999) 395–524.
[19] S.V. Patankar, Numerical heat transfer and fluid flow, John Benjamins Publishing Co., 1980. pp. 48–49.
[20] A. Dybbs, R.V. Edwards, A new look at porous media fluid mechanics-Darcy to turbulent, Fundam. Transport Phenomena Porous Media (1984) 199–254.